ROLE OF MODE MIXITY ON 3D STRESS VARIATIONS NEAR INTERFACIAL CRACKS

J.K. SINHA† and H.V. TIPPUR‡
Department of Mechanical Engineering
Auburn University, Alabama 36849, USA

ABSTRACT

The elasto-optic effects are mapped as $(\sigma_x + \sigma_y)$ contours near interfacial cracks in polymer-metal bimaterials using Mach-Zehnder interferometry. The stress fields are investigated when the crack planes are subjected to dominant tensile stresses and pure shear stresses. The optical measurements are examined in conjunction with companion finite element simulations for estimating the regions of dominant three dimensional stress variations near cracks. Results suggest that in the domain $(x, y > 0)$ the size of the region of dominant three dimensional effects is significantly smaller for the case of pure shear (for both positive and negative shears) when compared to the tensile stress dominated case for oscillation index $\epsilon > 0$. The optical data analyzed by incorporating these observations improve the accuracy of crack tip parameter estimation.

KEYWORDS

interfacial cracks, 3D effects, Mach-Zehnder interferometry, optical measurements, finite element simulations.

INTRODUCTION

One of the issues that has drawn attention in recent years is related to 3-D deformations near interfacial cracks. This has particular relevance when field quantities are used along with 2-D solutions for fracture parameters estimation. Due to the material property mismatch along an interface, three dimensional effects may be significantly different near the crack tip when compared to the homogeneous counterparts. Further, since interfacial cracks inherently undergo mixed-mode deformations, understanding the interaction between mode-mixity and the size of three dimensional zone is important. Recently, Nakamura (1991) performed 3-D finite element computations to investigate stress fields near interface cracks for the special case of oscillation index $\epsilon = 0$. He examined stresses very close to the crack front to determine the existence and the size of the so-called K-field. Barsoum and Chen (1991) numerically investigated the 3-D field near the an interface crack. They showed that the crack tip singularity at the free surface corner to depend on the Poisson's ratio. Lee and Rosakis(1993) numerically analyzed the extent of the near-tip 3-D zone in a tensile stress dominated bimaterial system. Their results indicate severe near tip three dimensionality around most of the near tip region (up to half of the specimen thickness) and extend all along the interface of width equal to one half sheet thickness. Pidaparti and Pontula (1995) have found that the rubber materials have much larger 3-D zones compared to their linear counterparts. They observed that the size of the region of dominant 3-D effects increase with material mismatch up to 3-6 times the thickness.

The current work is motivated by the fact that these 3-D interfacial crack investigations reported in the literature have been generally numerical and experimental investigations are currently lacking.

[0]†Graduate Student, ‡Associate Professor.

Further, the crack tip three dimensionality is addressed when cracks are subjected to predominantly tensile stresses. One of the prominent features of an interfacial crack being that it inherently undergoes mixed-mode deformations and failure response depends on the sense of the local shear, understanding the role of mode-mixity on interfacial crack tip three dimensionality is important for experimentally determining of fracture toughness - crack tip mixity relationships.

MACH-ZEHNDER INTERFEROMETRY (MZI)

MZI is a full-field, high resolution, real-time optical technique which provides interference patterns that represent contours of $(\sigma_x + \sigma_y)$ (thickness average values). The interferometer is shown schematically in Fig.1. The light source is a He-Ne laser beam expanded and collimated to approximately 50 mm diameter. The interferometer consists of a reference optical path 1 and a test optical path 2 created using two beam splitters ($BS1$ and $BS2$) and two first surface mirrors (M1, M2). The path lengths are nominally equal and the two beams are recombined after M2. The optics is aligned to get a uniform fringe on the image plane. A fracture specimen made of an optically isotropic transparent material is placed in the test path 2. The complex amplitude distributions, E_1 and E_2, corresponding to paths 1 and 2 when 50/50 beam splitters are used are,

$$E_1 = A_o e^{(ikl)}, \qquad E_2 = A_o e^{(ik[l+\delta l+(n_o-1)B])} \tag{1}$$

where l represents the nominal geometric length of the two paths 1 and 2, δl represents a constant difference in path lengths that may exist during the initial alignment, $k(= 2\pi/\lambda)$ is the wave number, n_o and B are the nominal refractive index and the nominal thickness of the test specimen, respectively. Here, A_o is the constant amplitude for both reference and object waves. The term $(n_o - 1)$ corresponds to the optical path difference S between the two beams due to the specimen. The resultant intensity distribution on the camera plane corresponding to the undeformed specimen is then, $I = (E_1 + E_2)(E_1 + E_2)^*$. Therefore,

$$I = 2A_o^2[1 + \cos k[\delta l + (n_o - 1)B]), \tag{2}$$

where $(\cdot)^*$ is the complex conjugate. For constructive interference on the image plane,

$$k[\delta l + (n_o - 1)B] = 2N\pi \qquad or, \qquad \delta l + (n_o - 1)B = N\lambda, \tag{3}$$

where N is the fringe order ($N = 0, \pm1, \pm2, ...,$). When the specimen undergoes deformation, E_2 becomes $E_2 = A_o e^{(ik[l+(n_o-1)B+\delta S])}$, where $\delta S(x, y)$ constitutes both $\delta B(x, y)$ (thickness change) and $\delta n_o(x, y)$ (refractive index change). Thus, the intensity distribution for the deformed specimen is given by,

$$I = 2A_o^2(1 + \cos k[\delta l + (n_o - 1)B + \delta S]). \tag{4}$$

Again, for constructive interference,

$$k[\delta l + (n_o - 1)B + \delta S] = 2N'\pi \qquad or, \qquad \delta S = (N' - N)\lambda = \mathcal{N}\lambda, \tag{5}$$

where $\mathcal{N} = (N' - N) = 0, \pm1, \pm2, ...$ From the above analysis it is clear that interference patterns represent contours of constant δS and the sensitivity of measurement is equal to λ per fringe. When loads are applied to the object, a combination of refractive index change (stress-optic effect) and thickness change (Poisson effect) constitute δS. The path difference can be related to the mechanical field under plane stress approximation (see, Tippur et al., (1991)), as follows:

$$\delta S = cB(\sigma_x + \sigma_y), \tag{6}$$

c being the elasto-optic constant for the material. For PMMA $c = -0.92 \times 10^{-10}$ m^2/N.

INTERFACIAL CRACK TIP FIELDS

Specimen Preparation: For this investigation, bimaterial specimens with a relatively large stiffness mismatch were made from model materials namely PMMA and aluminum. Two equal thickness (B = 6 mm) pieces were bonded along an edge using an adhesive consisting of methyl-methacrylate monomer (MMA) and a polymerizing agent at room temperature. The choice of the bond material provides a nominally bimaterial joint. The metallic surface was sand blasted prior to bonding to enhance bond strength. A soft, pliable Teflon tape was (approximately 50 μm thick) used to produce a sharp edge discontinuity by squeezing together the two halves of the specimen by an externally applied pressure during curing. Before testing, each specimen was optically examined in the MZI set-up under no-load condition to ensure that the interface was free from residual stresses.

Crack plane subjected to dominant tensile stress: First, crack tip stresses $(\sigma_x + \sigma_y)$ were mapped using MZI for the case when the crack plane was subjected to dominant tensile stresses. A three-point-bend configuration, as shown in Fig.2(a), was used for the purpose. The beam height (W) was 80 mm, the distance between the two supports was (L) 165 mm and crack length a was 25.4 mm (a/W=0.32). In view of the experimental difficulty for applying the load exactly on the interface, the load was applied at a small distance 12.5 mm away from the interface. The corresponding interference patterns for an applied load of 335 N is shown in Fig.2(b). Note that the interference patterns were seen only the $y > 0$ region. Each fringe increment corresponds to an optical path length change of 633 nm or a change of 1.1 MPa. The contours shown as dotted lines will be discussed later in this section.

To obtain an estimate of the size of the zone of dominant 3-D deformations near the crack tip, a complementary plane stress finite element analysis was carried out using ANSYS software package. The finite element model consisted of 2712 eight node plane stress quadrilateral elements and 8405 nodes (see Fig.3a). The crack tip region was discretized using a fine mesh with 1056 crack tip elements within $0.55B$ radius and 1776 elements within $2B$ radius from the crack tip. The inner most ring of elements were as small as $0.001a$, a being the crack length. The near tip mesh is shown in Fig.3(b). Singularity elements were not used near the crack tip. The elements in the region $y > 0$ and $y < 0$ were assigned material properties of PMMA (material-1) and aluminum (material-2). The model was subjected to three-point bending as was done in the experiments. A plot of non-dimensional $(\sigma_x + \sigma_y)$ from computations and singular field description are plotted as a function of (r/B) in Fig.3(c) along two directions. The match between the two results is within 2% of each other and demonstrates that the finite element discretization is fine enough to adequately capture the full-field singular behavior near the crack tip. Next, The $(\sigma_x + \sigma_y)$ contours with levels corresponding to the optical fringe orders were generated from the numerical results. A direct superposition of the experimental fringes and finite element contours around the crack tip is shown in Fig.2(b) (broken lines) in the region $y > 0$. As can be seen, the match between the two results is good in certain regions around the crack tip while significant departures are observed close to the interface, ahead and behind the crack tip. The agreement between the two results suggests that in those regions optical data adequately ($\pm$10% error) represent the plane stress behavior. On the other hand, disagreement between the two suggests the potential influence of 3-D variations in the stress fields, not captured by the plane stress FE simulations in the immediate vicinity of the crack tip. The agreement between the two results is seen to be good in the region approximately $r/B > 0.3$ (estimated nonlinear zone size is of the order of $r/B \approx 0.02$ in PMMA) and $65^o < \phi < 135^o$, where (r, ϕ) represent the crack tip polar coordinates. In fact, the fringes and the numerical contours are in excellent agreement between 90-130^o at much smaller radial distances. These observations are similar to the ones recently reported by Lee and Rosakis (1993) using finite element computations for a large stiffness mismatch bimaterial system. Next, these observations were quantified by defining error E_r as,

$$E_r = \left(\sigma_{\alpha\alpha}^{exp} - \sigma_{\alpha\alpha}^{FEA}\right)/\sigma_{\alpha\alpha}^{exp}, \qquad \alpha = x, y, \tag{7}$$

and $\sigma_{\alpha\alpha}^{exp}$ and $\sigma_{\alpha\alpha}^{FEA}$ correspond to experimental and and finite element values of stresses at a generic point in the field (summation over α is implied). The optical data was gathered along discrete directions where sufficiently large number of fringe intersections occur with a radial line drawn from the crack tip. The corresponding numerical data was also generated from the finite element output. Since finite element nodes do not generally coincide with the fringe locations, the two sets of data were fitted with curves and the fitted functions were used to calculate E_r at different $(r/B, \phi)$ values. In Fig.4(a) E_r is plotted as a function of normalized distance r/B from the crack tip along discrete directions. As observed earlier, the error plot suggests that the data along 120^o and 90^o

are within ±10% error band in the region beyond $r/B > 0.3$ while the error along 30° and 150° are in the range of 25-30%. Based on these observations in Fig.4(b) a region of dominant three dimensional effects (unshaded region) is shown. The shaded region in Fig.4(b), however, adequately represents plane stress behavior to within ±10% in $(x, y > 0)$. *It should be emphasized that in the shaded region K-dominant assumptions may still not be valid* and will be discussed later on.

Crack plane subjected to pure shear stress: The bimaterial specimens were loaded in asymmetric four-point-bending configuration to simulate pure shear conditions on the crack plane. The schematic of the specimen and the loading configuration is shown in Fig.5(a). In this configuration, by simply varying the distance s between the interface and the loading axis different applied loading mixities can be realized. When $s = 0$, the crack plane is under pure shear. Since, the crack tip deformations and the failure responses are distinctly different for the cases when the crack plane is subjected to 'negative' and 'positive' pure shears (see, Xu and Tippur, 1995), experiments were conducted for both $+s$ and $-s$ arrangements. The schematic in Fig.5(a) corresponds to $-s$ configuration (net shear force on the crack plane is in the $-x$ direction). Also, in this geometry the the mode-mixity of the applied loads on the interfacial plane is independent of the dimensions C and D (Xu and Tippur, 1995).

The asymmetric four-point-bend samples were subjected to pure negative and positive shear loadings. The corresponding optical maps of $(\sigma_x + \sigma_y)$ were obtained in the crack tip vicinity and are shown in Fig.5(b) and (c). As before, sensitivity of stress measurement is 1.1 MPa change between two successive (dark or light) fringes. Evidently, crack tip stress fields when pure shear is applied are quite pronounced behind the crack tip and relatively less spread-out ahead of the crack tip. Next, the previously described finite element model was subjected to asymmetric four-point-bend loading and the corresponding finite element fringes representing contours of $(\sigma_x + \sigma_y)$ were synthesized from the numerical data. The two contour maps were superposed for negative and positive shear cases and are shown in Fig.5(b),(c) (broken lines). As in the tensile stress dominated case, the agreement between the two results are excellent in certain regions while significant departures are evident in others. The agreement between the two results validates plane stress assumptions used in the computations while disagreement suggests zones where 3-D variations are significant. In both instances, in the region $r/B > 0.3$ and $30° < \phi < 150°$ good agreement between the experimental results and computations exist while the departures are significant elsewhere in $(x, y > 0)$. Once again, along the interface, 3-D effects are pronounced and hence a plane stress behavior has not taken hold in the neighborhood of the interface. These are further quantified in Figs.6(a),(b) where error E_r is plotted as a function r/B along discrete directions. Clearly, most of the radial directions outside $r/B > 0.3$ and $\phi = 30 - 120°$ clearly fall within ±10% error band. This suggests a much smaller zone of 3-D effects in case of pure shear (positive or negative) acting on the crack plane in $y > 0$ region. When the sense of the shear is positive on the crack plane, the interference patterns were such that only limited data could be gathered ahead of the crack and hence the error plots are limited to fewer directions. Based on these observations, a schematic of the region of potential 3-D effects is shown Fig.6(c) (unshaded region). As in Fig.3(b), the shaded region corresponds to locations where plane stress assumptions are satisfactory.

From the above it is clear that the estimated region of dominant 3-D effects based on tensile stress dominated simulation is rather conservative. However, the accuracy of crack tip parameters estimation using least-squares approach typically improves when the data are gathered from a larger region near the crack tip. In view of this, the current results are encouraging as it suggests that one could gather data from a much larger region when the imposed shear component on the crack plane is increased.

An independent verification of the same has also been carried out using 3-D FE simulations of the above cases. To quantify three dimensionality Rosakis and Ravi-Chandar (1986) have defined the so-called plane strain constraint $C_\epsilon = \sigma_z/\nu(\sigma_x + \sigma_y)$. Under plane stress conditions this parameter is zero and is equal to ±1 under plane strain conditions. Three dimensional stress analyses were performed separately for the tensile and shear dominated cases and the results are reported elsewhere (Sinha, et al., 1996). The three dimensional computations of C_ϵ support the experimental observations described earlier.

Extraction of Crack Tip Parameters from Optical Data: Considering the material above the interface $(0 < \phi < \pi)$, and following Rice (1988), the asymptotic expression for MZI fringes can be derived:

$$cB(\sigma_x + \sigma_y) = 4cB \sum_{n=1,3,5...}^{\infty} e^{\epsilon(\phi-\pi)} r^{(\frac{n}{2}-1)} \left\{ A_n \cos[(\frac{n}{2}-1)\phi - \epsilon \ln(\frac{r}{a})] + B_n \sin[(\frac{n}{2}-1)\phi - \epsilon \ln(\frac{r}{a})] \right\}$$
$$+ \frac{8cBc_2}{c_1+c_2} \sum_{n=2,4,6...}^{\infty} r^{(\frac{n}{2}-1)} \left\{ A_n \cos(\frac{n}{2}-1)\phi + B_n \sin(\frac{n}{2}-1)\phi \right\} = \mathcal{N}\lambda, \quad (8)$$

where $c_i = (\kappa_i+1)/\mu_i$, $\kappa_i = (3-\nu_i)/(1+\nu_i)$ for plane stress ($i = 1$ for PMMA and $=2$ for aluminum) and $\mathcal{N} = 0, \pm1, \pm2....$ denote fringe orders. A_n and B_n (n=1,2,3....) are the constant coefficients of the asymptotic expansion. Here μ and ν represent shear modulus and Poisson's ratio respectively, and,

$$\epsilon = \frac{1}{2\pi} \ln \frac{\mu_1 + \mu_2\kappa_1}{\mu_2 + \mu_1\kappa_2},$$

is the oscillation index. For the bimaterial under consideration ϵ=0.098 for plane stress. Note that, the complex stress intensity factor is related to A_1 and B_1 as follows,

$$(Ka^{i\epsilon}) = 2\sqrt{2\pi} \cosh(\pi\epsilon)(A_1 + iB_1).$$

The phase of $(Ka^{i\epsilon})$ $(= \tan^{-1} Im(Ka^{i\epsilon})/Re(Ka^{i\epsilon}))$ is the crack tip mode-mixity $\psi(a)$.

The fringe patterns in Figs.2 and 5 were digitized for obtaining fringe location (r, ϕ) and fringe order $(\mathcal{N})$ data. Only the data corresponding to the shaded region were used in the analysis. The fracture parameters were extracted using overdeterministic least-squares procedure. Also, K-dominant assumptions (eq.(9)) were relaxed during the analysis and higher order terms were incorporated in order to account for possible non-singular contributions to the field at distances beyond the anticipated 3-D zone. For example, the difference between the optical data and the least-squares fit in Fig.7(a) (for shear dominated case shown in Fig.5(b)) suggests possible influence of non-singular stresses to the crack tip field in regions beyond the estimated 3-D zone and a need for including higher order terms in the least-squares analysis. During the analysis, the higher order contributions were included sequentially until the match between in the least-squares fit and the data was satisfactory and, stable values of the dominant parameters was achieved. The result for the case when $n = 3$ in eq.(9) is shown in Fig.7(b). A good agreement between the least-squares fit and measured data is evident when higher order terms are incorporated into the analysis. Further details of the optical data analysis can be found in Sinha et al., (1996). The crack tip parameters obtained from the above analysis for all the cases considered in this paper are compiled in Table-1. The table also includes the FE counterparts using the codes developed in Xu and Tippur (1995). Good agreement between the optical measurements using the data in the shaded region for least-squares analysis (column-1) and finite element computations (column-2) are clearly evident. Further, the stress intensity factor results for these cases when all the digitized data points in both shaded and unshaded regions were used in the least-squares analysis (without taking into account potential 3-D stress variations) is also shown (column-3). The results in column-3 show poor correlation with the finite element computations. It should be emphasized that least-squares analyses of optical data are generally robust and do not show susceptibility to minor errors at individual data points. However, such an advantage does not exist when dealing with pointwise data in the field and 3-D effects such as the ones reported here could directly affect the error of the estimated parameter.

TABLE-1

	Experimental (data from shaded region)		Plane stress FEA		Experimental (data from shaded+unshaded regions)	
Loading	$Re(Ka^{i\epsilon})^{exp}$	$Im(Ka^{i\epsilon})^{exp}$	$Re(Ka^{i\epsilon})$	$Im(Ka^{i\epsilon})$	$Re(Ka^{i\epsilon})^{exp}$	$Im(Ka^{i\epsilon})^{exp}$
Pure shear (+)	-0.08	0.42	-0.10	0.38	-0.47	0.58
Pure shear (-)	0.30	-0.71	0.29	-0.69	0.39	-1.0
Tensile	0.58	0.13	0.56	0.06	0.77	0.13

CONCLUSIONS

An optical-finite element investigation of interface cracks in a large elastic mismatch bimaterial system suggests that mode-mixity affects the size of the region of three dimensional effects. The extreme cases of applied load mixities namely, predominantly tensile stress and pure shear stress (positive and negative), acting on the crack plane suggest that there is a significant reduction in the size of the region of 3-D effects in the latter when compared to the former in $y > 0$ for $\epsilon > 0$. That is, estimated zones of dominant 3-D effects based on former tends to be conservative for general situations of mixities for an interfacial crack. This is encouraging from the view point of experimental evaluation of fracture parameters using near tip measurements wherein data gathered from a larger region near the crack tip often improves the accuracy of parameter estimation. The regions where plane stress assumptions are adequate have been identified. By incorporating the experimental observations into the optical data analysis, fracture parameters have been accurately measured. Importance of avoiding data from the regions of dominant 3-D stress variations in experimental evaluation of crack tip parameters is demonstrated.

ACKNOWLEDGEMENTS

The research is supported by NSF Grant CMS-9313153.

REFERENCES

Barsoum R.S. and Chen, T. (1991). Three dimensional surface singularity of an interface crack. *Int. J. Fract.*, 50, 221-237.

Lee, Y.J. and Rosakis, A.J.(1993). Interfacial cracks in plates: A three dimensional numerical investigation. *Int. J. Solids and Struct.*. 30(22), 3139-3158.

Nakamura, T., (1991). Three-dimensional stress fields of elastic interface cracks. *J. Appl. Mech.*, 58, 939-946.

O'Dowd, N.P., Shih, C.F. and Stout, M.G.(1992). Test Geometries for Measuring Interfacial Fracture Toughness. *Int. J. Solids Struct.*, 29(5), 571-589.

Pidaparti R.M.V. and Pontula, G.(1995). Three-dimensional analysis of interface cracks in rubber materials. *Int. J. Fract.*, 68, 315-332.

Rice, J.R.(1988). Elastic Fracture Mechanics Concepts for Interfacial Cracks. *J. Appl. Mech.*, 55, 98-103.

Rosakis, A.J. and Ravi-Chandar, K.(1986). On Crack-Tip Stress State: An Experimental Evaluation of Three-Dimensional Effects, *Int. J. Solids and Struct.* 22(2), 121-134.

Shih, C.F. and Asaro, R.J., (1988). Elastic-plastic analysis of cracks on bimaterial interfaces: Part-I Small scale yielding, *J. Appl. Mech.*, 55, 299-316.

Sinha, J.K., Tippur, H.V., and Xu, L. (1996). An interferometric and finite element investigation of interfacial crack tip fields: Role of mode-mixity on 3-D stress variations. *Int. J. Solids and Struct.*, to appear.

Tippur, H.V. and Xu, L. (1996). Interfacial Crack Initiation under Quasi-static and Dynamic Loading Conditions: An Experimental Study. *Fatigue and Fracture of Engineering Materials and Strctures*, to appear.

Tvergaard, V., and Hutchinson, J.W., (1993). Influence of plasiticity on mixed-mode interface toughness, *J. Mech. Phys. Solids*, 41, 1119-1135.

Xu, L. and Tippur, H.V. (1995). Fracture Parameters for Interfacial cracks: An experimental-finite element study of crack tip fields and crack initiation toughness. *Int. J. Fract.*, 71: 345-363.

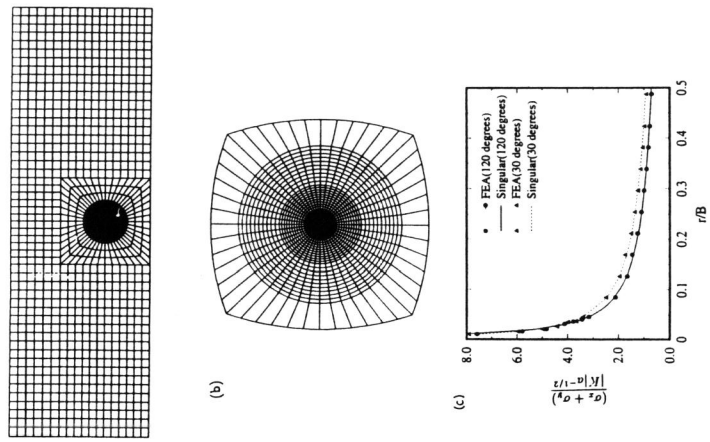

Figure-3: (a) Finite element mesh; (b) Near tip region, outer circle corresponds to r/B=2. (c) Comparison of stress fields between computations and singular descriptions.

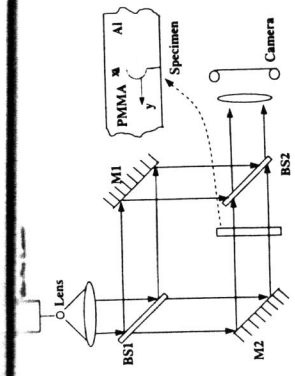

Figure-1: Schematic of Mach-Zehnder Interferometer.

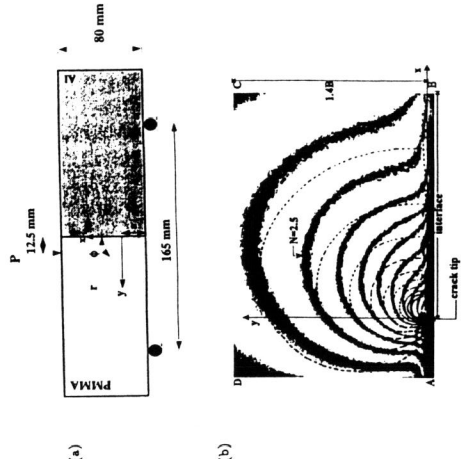

Figure-2: (a) Bimaterial specimen and 3-point bending configuration; (b) M2I fringes (contours of $\sigma_x + \sigma_y$) around the interfacial crack tip. (1.1 MPa/fringe; optical path change of $\lambda/2$ produces one-half fringe). Dotted lines from plane stress finite element simulation.

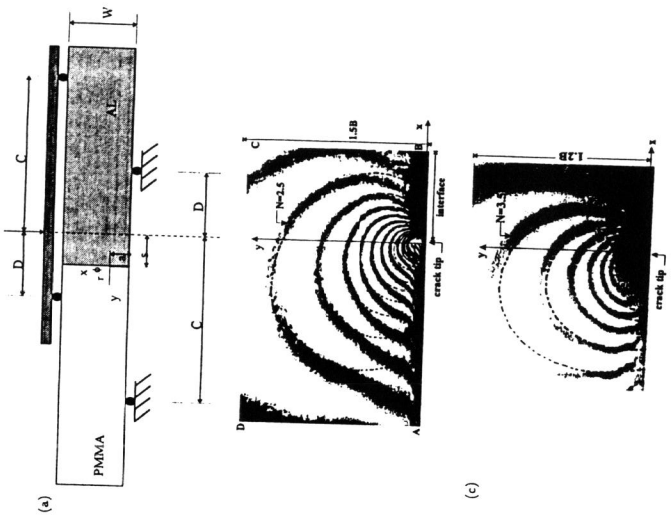

Figure-5: (a) Bimaterial specimen and asymmetric 4-point bending configuration ('negative' shear set-up). (b), (c) MZI fringes (contours of $\sigma_x + \sigma_y$) around the interfacial crack tip for 'negative' and 'positive' shear acting on the interfacial plane. Dotted lines represent corresponding FE contours.

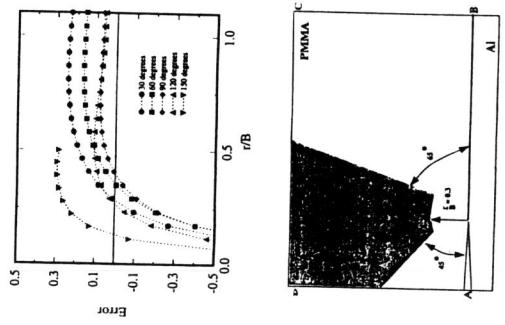

Figure-4: (a) Deviation between optical measurements and FE computations along different radial directions for 3-point bend specimen. (b) Regions of dominant three dimensional effects (unshaded region) and plane stress approximation (shaded region).

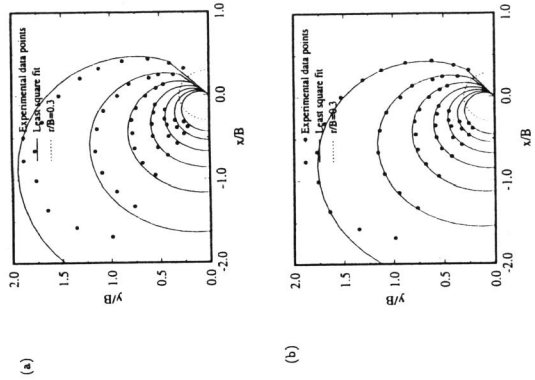

Figure-7: Least-squares analysis of optical data for the case of 'negative' shear loading on the interface plane: (a) with only K-dominant terms, (b) with asymptotic expansion with five constant coefficients.

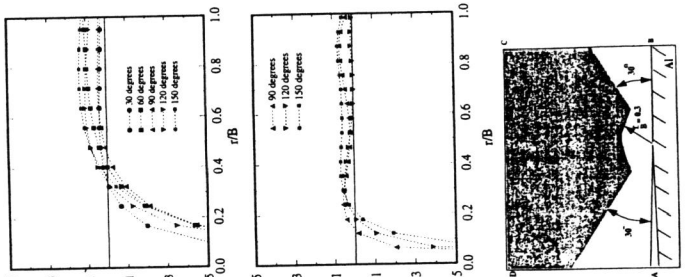

Figure-6: (a), (b) Deviation between optical measurements and FE computations along different radial directions for 'negative' and 'positive' pure shear on the interface plane. (c) Regions of dominant three dimensional effects (unshaded region) and plane stress approximation (shaded region).